Blood vessel network remodelling during tumor growth

M.Welter[a], H.Rieger[a,*]

[a] *Theoretische Physik, Saarland University, PF 151150, 66041 Saarbrücken, Germany*

Abstract

With the help of a theoretical model the process in which a growing tumor transforms a hierarchically organized arterio-venous blood vessel network into a tumor specific vasculature is analyzed. The determinants of this remodeling process involve the morphological and hydrodynamic properties of the initial network, generation of new vessels (sprouting angiogenesis), vessel dilation (circumferential growth), blood flow correlated vessel regression, tumor cell proliferation and death, and the interdependence of these processes via spatio-temporal changes of blood flow parameters, oxygen / nutrient supply and growth factor concentration fields. The emerging tumor vasculature is non-hierarchical, compartmentalized into well characterized zones, displays a complex geometry with necrotic zones and "hot spots" of increased vascular density and blood flow of varying size, and transports drug injections efficiently. Implications for current theoretical views on tumor-induced angiogenesis are discussed.

Keywords: Cancer; tumor growth; angiogenesis; vascular networks; blood flow; computer simulation

*Corresponding author Tel.: +49 681 302 3969; fax: +49 681 302 4899.
E-mail address: h.rieger@mx.uni-saarland.de (H.Rieger)

1 Introduction

Tumor vasculature, the blood vessel network supplying a growing tumor with nutrients like oxygen or glucose, is in many respects different from the hierarchically organized arterio-venous blood vessel network in normal tissues. In order to grow beyond a size of approximately 1-2 mm^3 the tumor has to switch to an angiogenic phenotype and to induce the development of new blood vessels mainly via sprouting angiogenesis, i.e. the formation of new vessels from pre-existing vasculature (Carmeliet and Jain 2000). This process is regulated by a variety of pro- and anti-angiogenic factors and as a consequence the anatomy of a solid, vascularized tumor grown within in a vascularized tissue displays a characteristic compartmentalization into essentially three regions (Holash et al. 1999a,b; Döme et al. 2002, 2007): i) The highly vascularized tumor perimeter with a microvascular density (MVD) that is substantially higher than the MVD of the surrounding normal tissue. ii) The well vascularized tumor periphery with dilated blood vessels and a tortuous vessel network topology. iii) A poorly vascularized tumor center with large necrotic regions threaded by only a few very thick vessels that are surrounded by a cuff of viable tumor cells.

Several microscopic phenomena on the cellular level have been identified to be involved in this remodeling process: 1) *Angiogenic sprouting:* Up-regulation of pro-angiogenic factors in tumor-cells (like vascular endothelial growth factor, VEGF, and other growth factors) can create additional vessels via sprouting angiogenesis in some regions of the tumor, most frequently in its perimeter (Carmeliet and Jain 2000). 2) *Vessel regression:* The maintenance of incorporated mature microvessels depends on the survival of endothelial cells (ECs) and their survival is intimately tied to their local microenvironment and, in particular, to the presence of pericytes, survival promoting cytokines, and extracellular matrix proteins. The major molecular players that control this process are angiopoietins and VEGF (Holash et al. 1999a,b), and in coopted blood vessels Ang-2 is up-regulated, causing the destabilization of their capillary walls, i.e the detachment of pericytes from the endothelial tube (Holash et al. 1999a,b). Once

ECs are separated from pericytes, they become particularly vulnerable resulting in the regression of destabilized vessels. *3) Vessel dilation:* The vascularization program of the pro-angiogenic phenotype can be switched from sprouting angiogenesis to circumferential growth in the interior of the tumor. This switch is mediated by the guidance molecules EphB4 (and its ligand ephrinB2), both expressed by ECs of malignant brain tumors (Erber et al. 2006), which acts as a negative regulator of blood vessel branching and vascular network formation, and also reduces the permeability of the tumor vascular system via activation of the Ang-1/Tie-2 systems at the endothelium/pericyte interface.

Besides pro- and anti-angiogenic molecular factors physical determinants like mechanical, hydrodynamical and collective processes are involved in the process that transforms or remodels the original arterio-venous blood vessel network into a tumor specific vasculature. Theoretical modeling can help to quantify the influence of the various factors determining this complex multiscale phenomenon. For recent reviews see (Tracqui 2009; Lowengrub et al. 2010, and references therein). Earlier work focusing on tumor induced angiogenesis can roughly be divided into three categories: 1) continuum models without a proper representation of a blood vessel network and blood flow (Balding and McElwain 1985; Chaplain and Stuart 1993; Chaplain et al. 1995; Byrne and Chaplain 1995; Holmes and Sleeman 2000), 2) hybrid models with a fixed vessel network geometry and a dynamically evolving tumor (Alarcon, Byrne and Maini 2003; Betteridge et al. 2006; Owen et al. 2008; Shirinifard et al. 2009), and 3) hybrid models with a fixed tumor (as a source of a diffusing growth factor) and a dynamically evolving tumor vasculature starting from a single parent vessel far away from the growth factor source (Anderson and Chaplain 1998; McDougall et al. 2002; Stephanou et al. 2005; McDougall, Anderson and Chaplain 2006). The latter models are also denoted as vessel-ingrowth models since the whole tumor vasculature grows from outside towards the tumor surface. Subsequent work was still inspired by these vessel-in-growth models (Zheng, Wise and Cristini 2005; Frieboes et al. 2007; Wise et al. 2008; Macklin et al. 2009): although in these studies the tumor also evolved dynamically, focusing on a detailed analysis of the

interactions between tumor and host tissue, all new vessels started to grow from one or more parent vessels in a non-physiologically far distance from the tumor. The remodeling process that transforms the original arterio-venous vasculature of the host tissue into a tumor specific vessel network has not been addressed with this Ansatz.

Bartha and Rieger (2006) hypothesized that the fundamental characteristics of the remodeling process and the emerging tumor vasculature is predicted by a model that comprises, besides the representation of a growing tumor, a sufficiently dense initial vasculature and three basic dynamical mechanisms - angiogenic sprouting, blood flow correlated vessel regression and vessel dilation. Indeed, the compartmentalization of the tumor as well other global features, like the time and radius dependencies of average MVD, tumor cell density, vessel radius and blood flow characteristics were predicted in good agreement with experimental data. These predictions were confirmed for varying grids in two space dimensions (2d) (Welter, Bartha and Rieger 2008) and three space dimensions (3d) (Lee, Bartha and Rieger 2006) as well as for arterio-venous initial vessel networks in 2d (Welter, Bartha and Rieger 2009) and 3d (Welter and Rieger 2010). For arterio-venous initial networks even local characteristics like the conditions for the formation of hot spots and spatial heterogeneities could be identified. In this chapter we want to survey these results for the dynamical evolution, final morphology and blood flow properties of tumor blood vessel networks and present a critical comparison of the various model variants.

2 Model definition

A network which is distributed homogeneously over the system domain serves as the initial vasculature for the model of remodeling by a growing tumor. Configurations based on regular lattices (Bartha and Rieger 2006; Lee, Bartha and Rieger 2006) akin to capillary beds as well as hierarchical organizations (Welter, Bartha and Rieger 2009) which mimic arterio-venous vasculatures were used. These networks are blood perfused and represent sources of oxygen.

Depending on the local oxygen concentration tumor cells represent the sources of the diffusion determined growth factor (GF) concentration field, which triggers either the generation of tip cells for angiogenic sprouting from existing vessels outside or at the periphery of the tumor, or circumferential growth within the tumor (for potential molecular mechanisms for this switch in the angiogenic program within the tumor see (Erber et al. 2006)). In contrast to vessel ingrowth models as in (Anderson and Chaplain 1998) tip-cells are not dominantly generated by branching of existing tip-cells but by sprouting from vessels of the original network. Lateral inhibition leads to a minimum spatial distance in a vessel segment between individual tip cell generation events (Bentley, Gerhardt and Bates 2008).

Tip cells migrate in the direction of a sufficiently large GF gradient (chemotaxis), otherwise randomly. The path they describe is supposed to be filled with stalk cells forming a lumen and finally, once the tip cell hits another vessel (anastomosis), a functional vessel carrying blood flow is formed. Due to the pre-existing vasculature vessels typically migrate only 50-100 μm before the filopodia of the tip-cell extending up to 20-30 μm into the surrounding tissue in all directions (Gerhardt et al. 2003) touch another vessel. Therefore directional cues are not as important here as in pure vessel in-growth models. Moreover, tip cells which fail to make successful contact with another vessel migrate maximally 100-150 μm and retreat afterward (Nehls, Herrmann and Hünken 1998).

Inside the tumor, vessels destabilize and regress (for the potential molecular determinants of this destabilization see (Holash et al. 1999a,b)). In our model an increasing contact time of vessels with tumor cells, implying an increasing residence time within the tumor, leads to a higher collapse probability of tumor vessels. The collapse probability is also correlated with the origin of the vessel (artery, vein or capillary) and the shear force exerted by the blood flow upon the vessel walls (Dimmeler and Zeiher 2000).

2.1 Configuration space

The state of the model is defined by the state of the discrete vessel network and the continuum fields for a non-specific growth factor concentration g, oxygen concentration o and tumor-cell density c.

The vessel network can be described as a graph where edges represent vessel segments and nodes represent potential branching points, respectively. This graph is embedded in a regular lattice with the lattice constant Δl, which means that the nodes are located at the lattice sites and edges are coincident with the lattice edges. Edges and Nodes are dynamically created and destroyed over time. In Addition they have attached dynamically varying biophysical properties

2.2 Blood flow

In order to determine blood flow, the edges of the network are regarded as ideal pipes with radius r, wall shear stress f and blood flow rate q. Consequently, q is determined by Poiseuille's law $q \propto r^4/\eta\Delta p$, where Δp is the hydrostatic pressure difference between the end points. The viscosity η is radius dependent, following Pries et al. (1994), for simplicity under the assumption of a homogeneous hematocrit of 0.45. Conservation of mass holds, meaning that the sum of all flow rates (with the appropriate sign) at each node must equal zero. With the addition of boundary conditions which in our model consist of prescribing the pressure p at some nodes, one obtains a well defined system of linear equations, which is solved numerically. The selection of these boundary nodes depends on the type of initial network. In arterio-venous networks the top-level root nodes are used (Welter, Bartha and Rieger 2009). In regular networks the pressure is prescribed at the system boundary to increase linearly from one corner of the domain to the opposite corner (Bartha and Rieger 2006)

2.3 Tumor cell density

In previous work Bartha and Rieger (2006); Lee, Bartha and Rieger (2006); Welter, Bartha and Rieger (2009) used a discrete cellular automaton model. There

individual tumor cells are represented as sites on a lattice and cell proliferation and tumor expansion are akin to eden growth with the additional constraint that sufficient oxygen must be available at proliferating sites. See the references above for a complete description.

Here and in (Welter and Rieger 2010) the model for the tumor is defined based on a continuum approach for the tumor cell density $c(\mathbf{r}, t)$. Under stress-free conditions without cell proliferation and death the tumor cell density is $c^{(norm)}$, which we assume to be $1/10$ μm^3 reflecting a typical lateral size of tumor cells of 10 μm. The dynamical evolution of the tumor cell density in the presence of cell proliferation and death is assumed to be given by a reaction-diffusion equation

$$\partial c/\partial t = -\nabla \cdot J + c^+ + c^- \ , \tag{1}$$

where J is the tumor cell flux and c^+ and c^- are source and sink terms describing cell proliferation and death, respectively.

In the following c^+,c^- and J are defined: We assume that tumor cells need sufficient oxygen to proliferate, which means that the local oxygen concentration o must exceed the threshold $o_{TC}^{(prol)}$, else $c^+ = 0$. Moreover we assume that a maximum packing density $c^{(max)}$ exists where cells are compressed so that they cannot proliferate further. We use the simplest expression to reflect that:

$$c^+ = 1/t_{TC}^{(prol)} c(1 - \frac{c}{c^{(max)}}) \quad \text{if } o \geq o_{TC}^{(prol)} \quad \text{else } 0 \ , \tag{2}$$

where $t_{TC}^{(prol)}$ is the mean proliferation time of unconstrained cells. Furthermore we assume cells undergo apoptosis with the constant death-rate $1/t_{TC}^{(death)}$ if the local oxygen level o drops below $o_{TC}^{(death)}$. The model includes this by the definition of c^-:

$$c^- = -1/t_{TC}^{(death)} c \quad \text{if } o < o_{TC}^{(death)} \quad \text{else } 0 \ . \tag{3}$$

For simplicity interaction with the resulting cellular debris is neglected. In the following the cell-flux J is defined. We assume that cells migrate only in response to compression. Therefore a phenomenological "solid pressure" P is introduced. Its equation of state depends on the cell density c as follows: Below the density

$c^{(norm)}$ cells are not compressed, thus feel no forces, thus we set $P = 0$ for $c \leq c^{(norm)}$. Else we define P as linear function which is zero for $c = c^{(norm)}$ and increases to $P = 1$ for $c = c^{(max)}$. In the style of Darcy's law, momentum terms in the equations of motion are neglected so that the cell migration speed is proportional to the driving force, which means that

$$J = -Dc\nabla P \,, \tag{4}$$

where D is an additional mobility constant. The cell density cannot exceed $c^{(max)}$ since there are no external forces and $c^+ \to 0$ for $c \to c^{(max)}$ even though P remains finite.

In the general framework of such a model it would be possible to add cell-cell adhesion. In this case one would consider volume fractions of other species e.g. normal tissue and necrotic tissue which interact via a free energy potential. See (Frieboes et al. 2007, and the references therein). The result is an effective surface tension force. Combined with expansive forces which drive the tumor rim outward it can cause a fingering instability. In our simpler model where we have omitted such forces, tumor cells move diffusively opposed to their density gradient. Since tissue oxygenization is homogeneous on a coarse scale this results in approximately spherically growing tumors. Biologically our model corresponds to a situation where tumor cells adhere to each other as much as to other cells. Also the tumor can expand without significant resistance from the surrounding tissue. We can justify this because (i) not all tumors exhibit fingering instabilities, (ii) we consider small tumor of less than 1 cm diameter and (iii) pH level changes can happen that kill normal cells.

Below we compare our results with experimental data from melanoma. To accommodate the model to this specific tumor type, which can extend through multiple skin layers from the surface to muscle tissue, it would be straight forward to include inhomogeneous and / or anisotropic environments. We would expect this to trigger a different front shape of the growing tumor. However we think – as is the case with a "fingering" tumor – that the characteristics of the blood vessel network in which we are interested would be invariant with respect

to such additions.

In order to identify necrotic regions, we record the maximum local TC density over time. If the current TC density is zero and there were TCs in the past, we consider the location to be necrotic. On the basis of the rest of our framework, there are no forces that would impose interesting dynamics on the shape of necrotic regions. Thus we use this crude approximation.

The equations are discretized with a simple explicit finite volume scheme on a cubic grid with 30 μm grid-cell size. We compute the fluxes through the cell faces separately. Knowing the fluxes, $\nabla \cdot J$ in (1) is discretized using a convective upwind scheme. To ensure stability, the time step for the integration is 0.1 h, whereas the updates of the rest of the system (see below) are done in 1 h steps.

2.4 Oxygen concentration field

The time scale for oxygen diffusion to reach a stationary state is of the order of seconds whereas the times scale for tumor cell proliferation, tip cell migration and endothelial cell proliferation is of the order of hours. Therefore we use for the oxygen concentration the quasi-static solution o of the diffusion equation, which adopts instantaneously any change in the source (vessels) and sink (tumor cells) configuration:

$$0 = \nabla^2 o - \gamma_o o + \alpha_o (o^{(B)} - o) \; , \tag{5}$$

where γ_o is a consumption rate coefficient, $o^{(B)}$ the blood oxygen level and α_o a source coefficient. γ_o is a linear combination of the tissue specific constants $\gamma_o^{(norm)}$, $\gamma_o^{(tum)}$ and $\gamma_o^{(necro)} = 0$, for normal tissue, tumor tissue and necrotic regions, respectively. The definition of the density parameters implies that necrotic areas inside the tumor do not consume oxygen. The factor α_o determines the amount of extravasated oxygen per concentration difference at the vessel wall. It is defined as permeability times wall surface area per concentration and tissue volume. For simplicity it assumes a constant value for all blood circulated vessels. $o^{(B)}$ is the oxygen concentration in blood plasma, for which local variations are also neglected.

The coefficients γ_o and α_o comprise the diffusion constant and therefore it does not appear in (5). We estimate γ_o based on the diffusion range R_o of oxygen around isolated vessels found in tumors. Therefor we use that a delta peak as source distribution generates an exponentially decaying radial profile $\exp(-x\sqrt{\gamma_o})$. Thus R_g is of the order of $1/\sqrt{\gamma_o}$. The parameter $o^{(B)}$ is determined such that, given γ_o, the concentration in between vessels is ca. 50% of the concentration at the vessel wall.

2.5 Growth factor concentration field

The growth factor concentration g is computed by a Greensfunction-like method. Underoxygenized tumor cells, which means that locally $o < o_{TC}^{(prol)}$, produce growth factor with a constant rate. It diffuses through the tissues and degrades with a constant rate. Therefore each source cell produces an exponentially decaying distribution. Thus we can write g as

$$g(\boldsymbol{x}) = \int d^3\boldsymbol{x\prime}\, G(||\boldsymbol{x\prime} - \boldsymbol{x}||)\, \theta(o_{TC}^{(prol)} - o(\boldsymbol{x\prime}))\, c(\boldsymbol{x\prime})\ , \tag{6}$$

where θ is the Heaviside step function. For simplicity we define $G(x) \propto \max(0, 1 - x/R_g)$ as a linearly decaying normalized function which vanishes at $x = R_g$, where R_g is a "diffusion range" and limits the region where angiogenesis is induced.

2.6 Vessel network remodeling dynamics

The evolution of the network is subject to three stochastical processes: sprout initiation, sprout migration and collapse as well as continuous wall degeneration and vessel dilation (Fig.1). The definition of these processes closely follows the definition in (Welter, Bartha and Rieger 2009), where 2d networks are considered. Therefore we only give a brief description here and refer in particular for the biological motivation of the details to (Welter, Bartha and Rieger 2009).

Sprout initiation: A new vessel segment can be added with probability $\Delta t/t_{EC}^{(sprout)}$ at any location on the network if the local growth factor concentration is

non-zero, the distance to the next branching point is less than $l^{(spr)}$ and the time spent within the tumor is less than $t_{EC}^{(switch)}$. "Within" the tumor is defined as $\langle c \rangle > c^{(norm)}/2$ averaged over the segment. The sprout segment occupies an edge on the lattice (length Δl) and points in the direction of the largest growth factor increase.

Sprout migration: These new segments are tagged as sprouts which has the following implications. Segments are appended to the current tip with probability $\Delta t / t_{EC}^{(sprout)}$, extending the original sprout. Sprouts can also spawn sub-sprouts like normal vessels can. But they are excluded from the collapse, degeneration and circumferential growth mechanisms. Sprouts are untagged and become normal vessels if the tip fuses with another vessel such that blood can flow, or if their respective life-time variable τ, which every sprout has attached, reaches its predefined maximum $t_{EC}^{(migr)}$. If the tip fuses with another sprout without creating a conducting branch, the involved segments remain tagged.

Wall degeneration: The structural support provided by the cell layers surrounding the endothelial cells is represented by the wall stability variable w. For new vessels and the original vasculature it is initialized with the wall-thickness of healthy vessels (Welter, Bartha and Rieger 2009). For vessels inside the tumor its value decreases at the constant rate Δw until zero.

Vessel collapse: A segment can be removed with probability $\Delta t / t_{EC}^{(coll)}$ if its wall stability variable w is zero and the wall shear stress f is below the threshold $f^{(coll)}$.

Vessel dilation: The vessel radius r increases at the constant rate k_r if $r < r^{(max)}$, the average growth factor concentration over the segment is non-zero and if the time spent within the tumor is larger than $t_{EC}^{(switch)}$.

Per time step ($\Delta t = 1$ h), a Monte-Carlo sweep is done per stochastical process and all continuous variables and fields are advanced in time. The pa-

rameter values that we use throughout the paper are given in table 1 (references to physiological data are given in (Bartha and Rieger 2006; Welter, Bartha and Rieger 2008, 2009).

The model is stable with respect to parameters since our observables vary smoothly with parameter deviations. For brevity we omit a analysis here. In previous papers Bartha and Rieger (2006); Welter, Bartha and Rieger (2008) discussed variations for 2d models which are also relevant for the present study.

2.7 Arterio-veneous tree construction

A normal vasculature is hierarchically organized. Arterial and venous trees provide the supply and drainage system for the capillary bed. Vessels in these trees divide into increasingly thinner branches like nearly ideal binary trees, with the exception of occasional anastomosis. Their terminal branches are connected to capillaries, which is where most of the exchange with the surrounding tissue occurs. Capillaries are accordingly thin, permeable and densely and homogeneously distributed. The design goal of such a structure is to provide a sufficient supply of nutrients to all regions of the tissue, while minimizing the energy necessary to maintain the circulation.

We follow Gödde and Kurz (2001) who presented a method to construct representations of vascular trees stochastically according to probabilistic rules that depend on local system properties. The construction of the blood vessel network is based on the stochastic remodeling of a collection of binary trees. Each tree represents either an arterial or a venous branch. Analogous to the definition Sec.2.1, the tree edges coincide with the edges of a lattice, and have associated hydrodynamic properties.

An initial "guess" for the network is constructed by a random growth process which originates from a prescribed set of arterial and venous "root" vessels or nodes located at the lattice boundaries. Thereby certain elementary structural elements are successively appended at randomly selected leaf nodes until the lattice is filled. The particular element and its direction is also selected randomly. Thereby moves, that would result in overlapping nodes are rejected.

For the study of 2d systems Welter, Bartha and Rieger (2009) used different root configurations with long stems positioned randomly within certain ranges. The structural elements comprised a single edge, and a Y-shape of three edges. See the above reference for detailed specifications.

For the 3d systems, single root nodes are uniformly distributed over the system domain faces. Arterial and venous types are selected in alternating order. Configurations are rejected, where the distance between two nodes or between a node and a domain edge is less than 10% of the domain lateral size. The growth pieces are selected from three planar configurations: a single edge, a $\dashv$ shape consisting of three edges, and a $-\sqsubset$ shape consisting of five edges. The latter two should approximate the more realistic Y shapes in real vasculatures.

After the initial growth successive optimization sweeps follow until a steady state evolves. Per sweep leafs are removed or extended depending on the wall shear stress in the parent edge. In order to determine a well defined blood flow (Sec.2.2), and also for the final output, the individual trees are temporarily connected by "capillary" edges between leaf nodes of opposing type (arterial or venous).

While it is highly non-trivial to synthesize vascular networks that are realistic in every way possible, our initial networks exhibit reasonable hierarchical structures, spatial distributions of the capillaries, and agreement with the flow-data in (Gödde and Kurz 2001) and the experimental references therein.

3 Temporal evolution

Fig.2 shows snapshots of the temporal evolution of the tumor and the vessel network for a 3d arterio-venous initial vasculature. Independent of the details of the initial vasculature and system dimensionality the emerging global morphologies share the same features. Initially the tumor oxygen consumption leads to decreased oxygen levels within the nucleus and consequently enables vascular remodeling via growth factor production of the TCs. The sprouting process first creates a dense capillary plexus which provides more oxygen and facilitates tu-

mor growth. Vessel collapses begin after a few days (Fig.2b). Small capillaries collapse immediately under bad perfusion while thicker vessels survive longer due to their stability (large w), independent on blood flow until they become unstable. The network is thus progressively remodeled, predominantly within a thin band around the tumor boundary. The sparse network left in the center remains static except for few collapses of isolated threads.

The resulting network morphologies shown in Fig.3 display the typical high-MVD periphery and low-density center. For the arterio-venous initial vasculatures, the remaining tumor vessels can form well perfused short-cuts between arteries and veins penetrating the tumor boundary. This is a consequence of the dilation that all vessels undergo in the tumor. The short-cuts consist of neovasculature as well as parts of the initial vasculature. For regular initial networks the surviving vessels are predominantly oriented along the global flow direction. This direction is imposed by the flow boundary conditions, dictating a homogeneous flow along the diagonal. Vessels perpendicular to this direction have lower flow rates and shear forces and are thus prone to collapse. Depending on parameters and the initial network configuration, arterio-venous systems can also exhibit such imposed flow directions between high-level arteries and veins. However this is much less apparent due to the hierarchical organization of the network. Starting with different initial arterio-venous networks yields different final configurations (Welter, Bartha and Rieger 2009) but their global characteristics, as quantified by the radial distribution functions analyzed in the following do not vary significantly.

The tumor masses grow approximately spherically. After a short initial phase their radius increases linearly since proliferation is predominantly restricted to the boundary where sufficient space and oxygen is available. The cell density profiles c exhibit steep slopes at at the invasive edges, dropping from $c^{(norm)}$ to zero. In the tumor interior c fluctuates between zero and $c^{(max)}$ depending on oxygenization. For the cellular-automaton based models (Bartha and Rieger 2006; Lee, Bartha and Rieger 2006; Welter, Bartha and Rieger 2009) the tumor cell density is constant and proliferation is limited to the outer rim by definition

and therefore these models also predict a constant expansion rate. Until ca. 300 h simulation time, the vessel network is still relatively dens so that all tumor cells are supplied with sufficient oxygen to remain viable ($o > o_{TC}^{(death)}$), but may not be able to proliferate ($o < o_{TC}^{(prol)}$). Further growth and an increasing number of vessel collapses lead to regions where the inter-vascular distance is greater than twice the oxygen diffusion radius. These regions become necrotic due to under-oxygenization and death of tumor cells.

In order to capture morphological and hydrodynamic characteristics quantitatively, we determined the average value of respective quantities in dependence on the radial distance r from the tumor center at different times. An example of these radial distributions is shown in Fig.4 for 3d arterio-venous systems. The data is averaged over 40 simulation runs with different initial networks and over concentric spherical shells centered around the tumor center.

The quantities of interest comprise the following: tumor density (in all panels), microvascular radius (MVR, panel a) microvascular density (MVD, panel b), blood flow rate through the vessels (q, panel c), vessel wall shear force (f, panel d), growth factor concentration (GF, panel f) and oxygen concentration (O_2, panel c) The microvascular density is defined as volume fraction occupied by the vessels. The quantities associated with vessel segments (MVR, f, q) are averaged over the number of vessel-occupied lattice sites within the respective shells.

The peak in the radial tumor density indicates the boundary of the tumor (stochastic fluctuations within the shells as well from sample to sample cause the finite width of this step). Since the individual curves are for equidistant times it is clear from the linear shift of the peak density that the tumor radius grows linearly in time. Behind the peak, at smaller distances r from the center, the tumor density drops monotonously, reflecting the emergence of necrotic zones in the tumor center.

The MVD in panel (b) of Fig.4 has a peak in the peritumoral region, i.e. outside of the tumor at a distance slightly larger than the peak of the tumor density. It is 1.5 to 2-fold higher than the normal MVD (plateau value at large

distances). Within the tumor (at small distances) the MVD drops monotonously to zero (at long enough times), again reflecting the emergence of the the necrotic core.

Correlated with the peak in the MVD is a small peak in the oxygen concentration (panel f of Fig.4), and a dip in the average vessel radius (panel a), the average flow rate (panel c), and the average shear force (panel d): The peak in the MVD in the peritumoral region reflects the presence of many new capillaries, which increase the oxygen supply but simultaneously decrease the average vessel radius since capillaries have minimum radius. Furthermore, since the average blood flow that is supplied by the arterio-venous network is approximately constant, this flow has to be distributed over 50-100% more microvessels in the tumor perimeter, which induces a reduction in average flow rate and shear force.

Within the tumor (i.e. for distances smaller than the location of the peak of the MVD) the vessel radius increases monotonously with decreasing distance from the tumor center (panel a of Fig.4), which is the effect of the switch from angiogenic sprouting to circumferential growth within the tumor. The axial blood-pressure gradient within the vessels dp/dl (not shown here) decreases monotonically with decreasing distance from the tumor center by more than one order of magnitude. Although the pressure gradient decreases, the average blood flow rate (q, panel c) within the vessels increases towards the tumor center since it is proportional to the 4th power of the vessel radius R, $q \propto R^4 dp/dl$. The average shear force f is proportional to the 1st power of R, $f \propto R\, dp/dl$, therefore it decreases with decreasing distance from the center.

The average oxygen concentration (panel f) decreases rapidly towards the tumor center and drops below the GF production threshold $o_{TC}^{(prol)} = 0.1$ (relative to normal oxygen) at approximately the same distance $r_{low\,oxy}$, where the the growth factor concentration (GF, panel f) displays a peak. This peak is therefore not at the same position as the peak of the tumor density. For distances smaller than the "underoxygenization radius" $r < r_{low\,oxy}$ all tumor cells produce GF and the shape of the GF concentration versus distance r is identical with the tumor density.

MVD and vessel-radius show the typical compartmentalization that has been observed in melanoma (Döme et al. 2002, 2007) and glioma (Vajkoczy and Menger 2000): For instance Döme et al. (2002) measured the MVD and vessel radius in three distinct regions of human and mouse melanoma: the central region, a 100 μm wide peripheral band just behind the invasive edge, a 200 μm wide peritumoral region outside the invasive edge. In the central region, they found a MVD that was reduced to 25% of the MVD of normal tissue, and increaesd up to 200% in the peritumoral region. They found that the vessel perimeter grew linearly from 50 μm to a plateau at 200 μm by day 15.

Analogous examinations were realized for 2d / 3d systems with regular initial networks (Bartha and Rieger 2006; Lee, Bartha and Rieger 2006) and 2d systems with arterio-venous network (Welter, Bartha and Rieger 2009), with qualitative and quantitative good agreement. The precise numbers might be different due to different parameters, minor model variations and initial networks. However the global characteristics such as the compartmentalization into regions of different MVD are also apparent.

4 Fractal dimension and spatial inhomogeneities

The topological and geometrical properties of tumor networks are vastly different from normal blood-vessel networks (Baish and Jain 2000). Tumor vessels are tortuous, lack a clear hierarchical organization and are spatially unhomogeneously distributed.

One can characterize and distinguish vessel networks by their are fractal properties. The concept of a fractal dimension is often used for this purpose (Gazit et al. 1995; Baish and Jain 2000). One commonly used method to estimate fractal dimension is box-counting, which is carried out by superimposing boxes of size ϵ arranged as a regular grid on the fractal object and counting the number of boxes N_ϵ which overlap the object. The self similar nature of true fractal object leads to the power law $N_\epsilon \propto \epsilon^{-D_f}$, where N_ϵ is the number of overlapping boxes. D_f is usually extracted by a linear fit in a log-log plot.

However due to the limited size and resolution of the data representation, determination of N_ϵ is limited to ca. two orders of magnitude of ϵ. Furthermore natural objects (or rather photographs thereof) are usually not perfectly fractal, giving rise to deviations from the ideal power law. Therefore even a small regime of a "good fit" is often considered sufficient to speak of a fractal dimension (or more truthfully named box-counting dimension); see the discussion in (Chung and Chung 2001).

The average dimension obtained from tumor networks based on 3d arterio-venous initial networks is $D_f^{av3d} = 2.50 \pm 0.02$. Tumor networks of 3d regular systems were analyzed by Lee, Bartha and Rieger (2006), who reported $D_f^{r3d} = 2.52 \pm 0.05$. For 2d arterio-venous systems we obtain $D_f^{av2d} = 1.79 \pm 0.03$ and lastly Bartha and Rieger (2006) reported $D_f^{r2d} = 1.85 \pm 0.05$. For brevity we refer to the references above and (Welter and Rieger 2010) for plots and additional data.

Bartha and Rieger (2006); Lee, Bartha and Rieger (2006) hypothesized that the fractal properties of the emerging tumor vasculature are independent of the initial (3d) blood vessel network. Our present finding that D_f^{av3d} of the tumor vasculature for a 3d arterio-venous initial network is close to D_f^{r3d} for 3d regular initial networks supports this hypothesis. For two dimensional systems the agreement between D_f^{av2d} and D_f^{r2d} is worse but within the margin of errors. Moreover D_f^{av3d} and D_f^{r3d} agree well with the exactly known value for the conventional critical percolation cluster in 3d $D_f^{perc3d} = 2.52$ (Stauffer and Aharony 1992). Analogously D_f^{r2d} is very close to the dimension of the percolation cluster in 2d $D_f^{perc2d} = 1.891$.

For sufficiently large systems such as the tumor networks based on 2d arterio-venous networks Welter, Bartha and Rieger (2009) could show that the fractal dimension of the tumor occupied region agrees well with the dimension of the tumor vessel network. The reason for this is that tumor cells survive everywhere in close proximity to vessels, which means that on a scale much larger than the diffusion radius of oxygen the shape of tumor is indistinguishable from the shape of the vessel network.

The basic mechanism responsible for the fractal properties of the tumor vasculature is the stochastic removal of vessels via vessel collapse and regression (Lee, Bartha and Rieger 2006; Welter, Bartha and Rieger 2008), see also (Paul 2009). In conventional percolation a critical cluster only emerges for an exactly tuned bond concentration. In our model the network is dynamically driven into this critical state without such a fine tuning since the removal of vessels is correlated with the blood flow: the collapse of weakly perfused vessels stabilizes the remaining ones due to an increase in blood flow. We propose that this mechanism, and not an underlying invasion percolation process (Baish and Jain 2000; Gazit et al. 1995; Baish and Jain 1998), is also at work in real tumors.

Moreover, spatial inhomogeneities were characterized by probability distribution functions (Fig.5) for (a) local MVD, (b) necrotic region size, and (c) size of regions with high MVD, where "high MVD" is defined as a local MVD which exceeds a fixed threshold value (ca. the MVD in normal tissue). The local MVD was determined as fraction of occupied sites within cells of a superimposed grid. For the central region of tumor networks emerging in 2d arterio-venous systems (Welter, Bartha and Rieger 2009), excluding the strongly vascularized periphery, the resulting distributions for (a),(b), and (c) show an algebraic decay with ca. the same exponent -1.4. The distribution for (a) also show a peak near zero, which is however trivial to due the existence of large necrotic regions. For 3d arterio-venous systems we obtain similar distributions which can also be fit by power laws but with significantly different exponents -0.5 (a), -1.9 (b) and -1.2 (c). These power laws are reminiscent of a self-organized critical state (Jensen 1998), for which the absence of a typical length scale (over which for instance size distributions would decay exponentially) is characteristic, like in a stochastic dilution process at the percolation threshold or a flow-correlated percolation process (Bartha and Rieger 2006).

In the following paragraphs we analyze the occurrence of so called "Hot spots". These hot spots are regions of increased blood flow within the tumor. In clinical imaging of blood flow they can be observed using tomography techniques. See e.g. (Pahernik et al. 2001). Since blood flow is directly linked to the

existence of blood vessels, it is also important to analyze spatial inhomogeneities of the tumor networks in order to understand "Hot spots". Furthermore the quantity q, defined in Sec.2.2 as blood flow rate of a vessel segment, is not directly experimentally accessible since it represents the total volume per time transported through a finite sized pipe which might contribute to several voxels in imaging data. The more relevant quantity is therefore the blood flow velocity (magnitude), which can be interpreted as spatially varying field.

For regular initial networks Bartha and Rieger (2006); Lee, Bartha and Rieger (2006) obtained tumor networks which consisted predominantly of isolated strings within the tumor center. It is possible to interpret even one of these strings as "Hot-spot" if there are no other blood perfused vessels in the close vicinity. Depending on parameters the blood flow velocity in these strings may be higher or lower than in the surrounding normal network. This is a consequence of the vessel dilation effect. Although it is the blood pressure which is prescribed via boundary conditions, instead of the blood flow rate, it can be assumed that the flow rate into the tumor is limited by the relatively high flow resistance of the capillary-like surrounding network. Therefore if the increase in blood capacity is not counterbalanced by sufficient vessel collapses (determined by the critical shear-stress parameter $f^{(coll)}$), the flow velocity in tumor vessel can be lower than in the original vasculature.

(Welter, Bartha and Rieger 2008) reported the possible emergence of morphological artifacts in systems with regular, hexagonal, initial networks. Therein surviving vessels converge to a singular point in the center of the tumor. On each side of the central point, perpendicular to the flow direction, a massive region void of vessels emerged. However, it should be stressed that the predicted global properties nonetheless agree with the results from other systems as presented in Sec.3. Moreover, these artifacts cannot occur in systems based on hierarchical arterio-venous networks due to the fundamentally different blood-flow boundary conditions and network organization.

Welter, Bartha and Rieger (2009) quantified and analyzed the spatial distribution of blood flow for 2d initial networks and Welter and Rieger (2010)

for 3d networks. In good agreement one could observe that some vessels form short-cuts between high-level arteries and veins penetrating the tumor rim. The dilation effect decreases the flow resistance of the thinnest vessels which would otherwise dominate the resistance of a potential short-cut. Which therefore leads to flow rates and velocities which are orders of magnitudes higher than in a normal capillary beds. The model thus supports the hypothesis raised in (Pahernik et al. 2001) that hot spots are due to highly conductive arterio-venous shortcuts. See the references above for plots of flow rate distributions. Also see Fig.7 and corresponding figures in the references for an impression of the transport or flow velocities.

Moreover, the model for 2d arterio-venous systems predicts the formation of dense clusters of surviving vessels in the tumor center, accompanying the predominant isolated strings. It could be shown that these clusters are more likely to form in regions with high hydrodynamic pressure differences between neighboring vessels. A spatially varying field $p(\mathbf{r})$ of these pressure differences can be constructed by determining the solution of the Laplace equation for $p(\mathbf{r})$ defined on the space between the vessels with the boundary condition that $p(\mathbf{r})$ is identical to the blood pressure inside the vessel at location $\mathbf{r}$. Thus, the field $p(\mathbf{r})$ interpolates the pressure between vessels (Fig.6). Correlations between the gradient magnitude $|\nabla p|$ of this map for the original vasculatures and the microvascular density in the emerging tumors were determined in two ways (Welter, Bartha and Rieger 2009): (1) Globally, where $|\nabla p|$ and the MVD were averaged over the region occupied by the final tumor for 40 different simulation runs. The resulting correlation coefficient is ca. 0.9. (2) Locally, where data points were generated by averaging over several sub-domains of 150 μm radius. Their correlation coefficient varies between 0.2 and 0.4, depending on parameters. Since single collapse events lead to long-ranged collapses of adjacent network sections, we think that therefore local measurements show significantly weaker correlations.

In contrast, dense vessel clusters observed in 2d are not apparent in the tumor vasculature emerging within the 3d arterio-venous networks. Concomitantly the

the pressure (gradient) fields for the 3d initial networks considered here are more homogeneous, except on a very short scale in between neighboring vessels. This is exemplified by Fig.6a in comparison to Fig.6b and c. We think that this is the consequence of the much larger configuration space for 3d initial networks compared to 2d. Vessels can wind around each other, arteries and veins can "cross" each other, which they cannot in 2d, etc. Therefore, using a stochastic algorithm, it seems to be very unlikely to construct a configuration which has the same particular properties as most 2d networks have.

5 Drug transport

Normal arterio-venous vessel networks are designed to transport a plenitude of substances efficiently to all regions within a tissue. The drastic differences between the architecture of tumor networks to normal networks, i.e. sparsity, tortuosity, lack of a clear hierarchy, etc., raises the question whether the morphological characteristics of tumor networks pose a problem to successful drug delivery. McDougall et al. (2002) first treated this question with the help of a simulation model, where a time-dependent concentration profile c over the vasculature is propagated according to the local blood flow-velocities.

The basis of this model is a network according to the definition in Sec.2.1 and 2.2. In addition, a mass parameter m is associated with each vessel describing the amount of drug within its blood volume. This mass m is deterministically updated in successive time steps: First the amount flowing out of vessels is determined and added to auxiliary mass variables associated with the network nodes. Under the assumption of perfect mixing, these nodal masses are then redistributed into further downstream vessel. A detailed description can be found in (Welter, Bartha and Rieger 2008; McDougall et al. 2002). For simplicity the exchange of drug with extra-vascular space has been neglected up till now.

The results presented by McDougall et al. (2002) and in subsequent papers (McDougall, Anderson and Chaplain 2006, and the references therein) are derived from a vascularization model of pure in-growth and are discussed in the

context of our results further below.

The transport model was adopted by Welter, Bartha and Rieger (2008, 2009); Welter and Rieger (2010) to check whether there are obstacles to successful drug delivery inherent to tumor network which are embedded in a surrounding normal vasculature. The studied systems comprised regular 2d, arterio-venous 2d and arterio-venous 3d initial networks, respectively.

The simulation starts with a "clean" network without drug. Drug is inserted with a constant dimensionless volume-concentration of value 1 simultaneously through the inlet nodes of the network. In the regular networks, these nodes comprise the boundary nodes of the network pattern where the (negative) pressure gradient imposed by the flow-boundary conditions (see Sec.2.2) points into the system domain. The resulting drug "front" advances relatively even through the entire network. Within the order of 60 s the front traversed to the out-flow nodes at the opposite corner of the domain, where the domain size is 12 mm and the diameter of the tumor is ca 6 mm. For continuous infusions the network is saturated with the maximum drug concentration after expiration of this time.

The results obtained for arterio-venous initial networks are similar thereto. When drug is inserted through all arterial inlets, it is distributed very rapidly over the whole network. Within the order of several seconds the network is saturated with the maximum drug concentration. To illustrate that, Fig.7 shows a sequence of snapshots over 4 seconds. At the tumor border, where the MVD is high and the networks contains many loops, there may be tiny regions (ca. 100 μm diameter) that take an order of magnitude longer to fill. Transport through the dilated tumor-internal vessels is as fast as through high-level vessels of the normal vasculature. The outer regions of the system where the network remains normal can also transport drug towards the tumor periphery. Therefore the tumor vasculature as a whole is well perfused. Qualitatively and quantitatively the results for 3d systems (Welter and Rieger 2010) and 2d systems (Welter, Bartha and Rieger 2009) are in good agreement. A notable exception seems to be the robustness of the initial networks with respect to the disruption by the tumor network. With this we mean that in 2d there are larger regions than in

3d ($\gg$ 100 μm diameter, extending into sections of the original network) with significantly decreased flow velocities. We presume this might be because the initial 2d configurations have fewer pathways to major feeding vessels. Therefore blood flow is more likely to traverse the comparably badly conducting tumor boundary, resulting in low flow rates.

Qualitatively it was for instance determined how long tumor vessels are exposed to a drug concentration larger than a predefined minimum drug level c_{thres}. Welter and Rieger (2010) report that during a 30 s simulation time over 90% of the vessel network was exposed to at least $c = 0.5$ for at least 25 s, and 99% for at least 15 s. Also by comparing exposure times for different c_{thres} they could conclude that drug advances through the network with a sharp front, exposing vessels "on contact" instantly to high drug concentrations.

Our conclusion is therefore that experimentally observed deficiencies in drug delivery must have other reasons, and these most probably lie within the characteristics of extravasation of drug and interstitial fluid transport within the tumor, which were not included into the present versions of the model.

6 Conclusion

We have demonstrated that realistic morphological properties of vacular remodelling in spherically growing solid tumors are correctly predicted by a methematical model involving a physiologically relevant initial vasculature and the dynamical processes of angiogentic sprouting in the tumor periphery, circumferential vessel growth and blood flow correlated vessel regression within the tumor. The emerging tumor vasculature is non-hierarchical and compartmentalized into a highly vascularised tumour perimeter, a tumour periphery with large vessels density and dilated vessels and a central region containing necrotic regions with a low microvascular density threaded by extremely dilated vessels.

The incorporation of an arterio-venous initial vascualture is important since it provides a mechanism for short-cuts or "shunts" and concomitantly an increased blood flow through the tumour vasculature (Welter, Bartha and Rieger

2009; Welter and Rieger 2010) as observed in experiments (Sahani et al. 2005): Thick arterioles and venules provide a well conducting support structure around the tumour. Since the total pressure difference between the tree roots is fixed, the transported blood volume is given by the total flow resistance of entire vascular tree. Dilation of a few vessels forming a path between the tree roots can remove bottlenecks formed by thinner vessels. The creation of new vessels thereby promotes arterio-venous short-cuts, or shunts, through multiple partly disjoint paths. After vessel dilation this leads to a decreased total flow resistance, which implies an increased blood flow through the tumour vasculature when compared with the initial vasculature. This is in contrast to grid-like initial networks, where the total flow resistance is dominated by the network outside the tumour (Bartha and Rieger 2006; Lee, Bartha and Rieger 2006; Welter, Bartha and Rieger 2008) and the flow cannot not increase via the dilation of tumour internal vessels. Moreover, depending on the details of their construction arterio-venous networks display characteristic spatial inhomogeneities that can, via locally increased pressure gradients (Welter, Bartha and Rieger 2009) or simply the presence of major arteries (Welter and Rieger 2010), lead to the formation of hot spots (i.e. regions of increased blood flow) inside the growing tumor.

Vessel dilation via circumferential growth within the tumor is a major physical determinant of the emerging network morphology and blood flow organization: Since blood flow through cylindrical vessels increases with the 4th power of its radius a single or a few dilated vessels can carry most of the blood entering a particular region of the tumor thereby destabilizing large parts of the capillary network.

The correlation of vessel regression with the shear force exerted by the blood flow upon the vessel walls is critical for the global geometry of the emerging tumor vasculature as well as for the blood borne drug transport: the basic mechanism responsible for the fractal properties of the tumor vasculature in our model is the stochastic removal of vessels via vessel collapse and regression. In conventional percolation Stauffer and Aharony (1992) a critical cluster only

emerges for an exactly tuned bond concentration. In our model the network is dynamically driven into this critical state without such a fine tuning since the removal of vessels is correlated with the blood flow: the collapse of weakly perfused vessels stabilizes the remaining ones due to an increase in blood flow. In addition the remaining vessels are all well perfused and as a consequence blood borne drug transport through the tumor vasculature is efficient, in contrast to vessel-in-growth models (McDougall et al. 2002; McDougall, Anderson and Chaplain 2006).

This does however not automatically imply that drug reaches all tumor cells since neither drug transport through the tumor tissue nor drug uptake have been addressed (Minchinton and Tannock 2006). The low differences between interstitial fluid pressure (IFP) and microvascular pressure (MVP) due to vessel leakiness (Hassid et al. 2006), causing low convection rates, as well as the low diffusibility of drug molecules through vessel walls, causing lower diffusion ranges for drug than for oxygen, appear to be the key physical determinants preventing successful drug delivery in tumors. Work that incorporates these mechanism in the type of models presented here is in progress.

References

Alarcon T, Byrne H, Maini P (2003) A cellular automaton model for tumour growth in inhomogeneous environment. J. Theor. Biol., 225, 257–274.

Anderson A R A, Chaplain M A J (1998) Continuous and Discrete Mathematical Models of Tumor-induced Angiogenesis. Bull. Math. Biol. 60:857–900.

Baish J W, Jain R K (1998) Cancer, angiogenesis and fractals. Nat. Med. 4:984.

Baish J W, Jain R K (2000) Fractals and cancer. Cancer Res. 60:3683–3688.

Balding D and McElwain D L S (1985) Mathematical modelling of tumour-induced capillary growth. J. Theor. Biol. 114:53–73.

Bartha K, Rieger H (2006) Vascular network remodeling via vessel cooption, regression and growth in tumors. J. Theor. Biol. 241:903–918.

Bentley K, Gerhardt H, Bates P A (2008) Agent-based simulation of notch-mediated tip cell selection in angiogenic sprout initialisation. J. Theor. Biol. 250:25–36.

Betteridge R, Owen M R, Byrne H M, Alarcon T, Maini P K (2006) The impact of cell crowding and active cell movement on vascular tumour growth. Netw. Hetero. Media 1:515–535.

Byrne H M, Chaplain M A J (1995) Mathematical models for tumour angiogenesis: numerical simulations and nonlinear wave solutions. Bull. Math. Biol. 57:461–486.

Carmeliet P, Jain R K (2000) Angiogenesis in cancer and other diseases. Nature 407:249–257.

Chaplain M A J, Stuart A M (1993) A model mechanism for the chemotactic response of endothelial cells to tumour angiogenesis factor. IMA J. Math. Appl. Med. Biol. 10:149–168.

Chaplain M A J, Giles S M, Sleeman B D, Jarvis R J (1995). A mathematical model for tumour angiogenesis. J. Math. Biol. 33:744–770.

Chung H-W, Chung H-J (2001) Correspondence re: Baish J W, Jain R K (2000) Fractals and Cancer. Cancer Res. 60:3683–3688. Cancer Res. 61:8347–8351.

Dimmeler S, Zeiher A M (2000) Endothelial cell apoptosis in angiogenesis and vessel regression. Circ. Res. 87:434–439.

Döme B, Paku S, Somlai B, Tímár J (2002) Vascularization of cutaneous melanoma involves vessel co-option and has clinical significance. J. Path. 197:355–362.

Döme B, Hendrix M, Paku S, Tóvári J (2007) Alternative Vascularization Mechanisms in Cancer. Am. J. Path. 170:1–15

Erber R, Eichelsbacher U, Powajbo V, Korn T, Djonov V, Lin J, Hammes H-P, Grobholz R, Ullrich A, Vajkoczy P (2006) EphB4 controls blood vascular morphogenesis during postnatal angiogenesis. EMBO 25:628–641.

Frieboes H B, Lowengrub J S, Wise S, Zheng X, Macklin P, Bearer E, Cristini V (2007) Computer simulation of glioma growth and morphology. NeuroImage. 37:59–70.

Furuberg L, Feder J, Aharony A, Jossang T (1988) Dynamics of Invasion Percolation. Phys. Rev. Lett. 61:2117–2121.

Gazit Y, Berk D A, Michael Leunig L T B, Jain R K (1995) Scale-invariant behavior and vascular network formation in normal and tumor tissue. Phys. Rev. Lett. 75:2428–2431.

Gerhardt H, Golding M, Fruttiger M, Ruhrberg C, Lundkvist A, Abramsson A, Jeltsch M, Mitchell C, Alitalo K, Shima D, Betsholtz C (2003) VEGF guides angiogenic sprouting utilizing endothelial tip cell filopodia. J. Cell Biol. 161:1163–1177.

Gödde R, Kurz H (2001) Structural and Biophysical Simulation of Angiogenesis and Vascular Remodeling. Dev. Dyn. 220:387-401.

Hassid Y, Furman-Haran E, Margalit R, Eilam R, Degani H (2006) Noninvasive magnetic resonance imaging of transport and interstitial fluid pressure in ectopic human lung tumors. Cancer Res. 66:4159–4166.

Holash J, Maisonpierre P C, Compton D, Boland P, Alexander C R, Zagzag D, Yancopoulos G D, Wiegand S J (1999a) Vessel Cooption, Regression, and Growth in Tumors Mediated by Angiopoietins and VEGF. Science 284:1994–1998.

Holash J, Wiegand S, Yancopoulos G (1999b) New model of tumor angiogenesis: dynamic balance between vessel regression and growth mediated by angiopoietins and VEGF. Oncogene 18:5356–5362.

Holmes M J, Sleeman B D (2000) A mathematical model of tumour angiogenesis incorporating cellular traction and viscoelastic effects. J. Theor. Biol. 202:95–112.

Jensen H J (1998) Self-Organized Criticality: Emergent Complex Behavior in Physical and Biological Systems. Cambridge University Press, Cambridge.

Lee D S, Bartha K, Rieger H (2006) Flow correlated percolation during vascular remodeling in growing tumors. Phys. Rev. Lett. 96:058104-1–058104-4

Lowengrub J S, Frieboes H B, Jin F, Chuang Y-L, Li X, Macklin P, Wise S M, Cristini V (2010) Nonlinearity 23:R1–R91

Macklin P, McDougall S, Anderson A R A, Chaplain M J, Cristini V, Lowengrub J (2009) Multiscale modelling and nonlinear simulation of vascular tumour growth. J. Math. Biol. 58:765-798

McDougall S R, Anderson A R A, Chaplain M A J, Sherrat J A (2002) Mathematical modelling of flow through vascular networks: implications for tumour-induced angiogenesis and chemotherapy strategies. Bull Math Biol. 64:673–702.

McDougall S R, Anderson A R A, Chaplain M A J (2006) Mathematical Modelling of dynamic adaptive tumour-induced angiogenesis: Clinical implications and therapeutic targeting strategies. J. Theor. Biol. 241:564–589.

Minchinton A I, Tannock I F (2006) Drug penetration in solid tumours. Nat. Rev. Canc. 6:583-592.

Murray C D (1926) The physiological principle of minimum work: The vascular system and the cost of blood volume. Proc. Natl. Acad. Sci. USA. 12:207–214.

Nehls V, Herrmann R, Hühnken M (1998) Guided migration as a novel mechanism of capillary network remodeling is regulated by basic fibroblast growth factor. Histochem. Cell. Biol. 109:319–329.

Owen M R, Alarcon T, Maini P K, Byrne H M (2008) Angiogenesis and vascular remodelling normal and cancerous tissues. J. Math. Biol. 58:689-721.

Pahernik S, Griebel J, Botzlar A, Gneiting T, Brandl M, Dellian M, Goetz A E (2001) Quantitative imaging of tumour blood flow by contrast-enhanced magnetic resonance imaging. Brit. J. Canc. 85:1655–1663.

Paul R (2009) Eurp. Phys. J. E. Flow-correlated dilution of a regular network leads to a percolating network during tumor-induced angiogenesis 30:101–114.

Pries A R, Secomb T W, Gessner T, Sperandio M B, Gross J F, Gaehtgens P (1994) Resistance to blood flow in microvessels in vivo. Circ. Res. 75:904–915.

Sahani D V, Kalva S P, Hamberg L M, Hahn P F, Willett C G, Saini S, Mueller P R, Lee T Y (2005) Assessing tumor perfusion and treatment response in rectal cancer with multisection CT: initial observations. Radiology 234:785–792.

Sheppard A P, Knackstedt M A, Pinczewski W V and Sahimi M (1999) Invasion percolation: new algorithms and universality classes. J. Phys. A 32:L521-L527.

Shirinifard A, Gens J S, Zaitlen B L, Poplawski N J, Swat M, Glazier J A (2009) 3D multi-cell simulation of tumor growth and angiogenesis. PLoS One. 4:e7190

Stauffer D, Aharony A (1992) Introduction to percolation theory. 2nd ed. Taylor & Francis, London.

Stephanou A, McDougall S R, Anderson A R A, Chaplain M A J (2005) Mathematical modeling of flow in 2D and 3D vascular networks: applications to anti-angiogenic and chemotherapeutic drug strategies. Math. Comput. Model. 41:1137–1156.

Tracqui P (2009) Biophysical models of tumour growth. Rep. Prog. Phys. 72:056701–056731

Vajkoczy P, Menger M D (2000) Vascular microenvironment in gliomas. J. Neurooncol. 50:99–108.

Welter M, Bartha K, Rieger H (2008) Emergent vascular network inhomogeneities and resulting blood flow patterns in a growing tumor. J. Theor. Biol. 250:257–280.

Welter M, Bartha K, Rieger H (2009) Vascular remodelling of an arterio-venous blood vessel network during solid tumour growth. J. Theor. Biol. 259:405–422.

Welter M, Rieger H (2010) Physical determinants of vascular network remodeling during tumor growth. Eur. Phys. J. E., in press.

Wise S M, Lowengrub J S, Frieboes H B, Cristini V (2008) Three-dimensional multispecis nonlinear tumor growth – I Model and numerical method. J. Theor. Biol. 253:524–543.

Wu J, Long Q, Xu S X, Padhani A R (2009) Study of tumor blood perfusion and its variation due to vascular normalization by anti-angiogenic therapy based on 3D angiogenic microvasculature. J. Biomech. 42:712–721.

Zheng X, Wise S M, Cristini V (2005) Nonlinear simulation of tumor necrosis, neo-vascularization and tissue invasion via an adaptive finite-element/level-set method. Bull. Math. Biol., 67:211–259.

Figure 1: Illustration of the vessel network remodeling processes. The contents of the boxes display exemplified states of the vessel network. The vessel segments are shown as blue boxes if perfused with blood, else they are in a gray shade. The dark-blue borders represent vessel walls of varying thickness and detached cells (in c). The presence of a tumor is hinted at by a yellow mass. The state transitions go from left to right as indicated by the arrows, whereby the rate parameter is denoted below- and essential preconditions above the arrows. In (a) a new sprout is generated by potentially splitting an existing segment, adding a node and adding the new sprout segment. In (b) the sprout is extended by adding further segments to its tip. (c) Vessel walls degenerate within the tumor due to detachment of support cells. This is modeled by a decreasing maturation parameter and depicted here as decreasing wall strength and surrounding debris. (d) Vessel regression is modeled by removal of segments with critically low shear-force (indicated by the red segment). This can disrupt blood flow over large sections, leaving many non-circulated vessels, which will also regress within a very short time scale. (e) Within the tumor vessels dilate. (See text for details.)

Figure 2: Visualization of 3d vessel network and tumor configurations obtained at times 100 h (a), 200 h (b), 400 h (c), and 500 h (d), based on an arterio-venous initial network. A cut through the cubic simulation volume is shown. The scale bar represents approximately 1 mm. The vessels are depicted as cylinders which are color coded by their blood flow rate q. On a logarithmic scale, it reaches from 1 (green) over 10^6 (blue) to 10^9 (red) in units of $\mu\mathrm{m}^3/\mathrm{s}$. Non-circulated vessels are shown in gray shades. The spheroid in the center shows the iso-surface where the tumor cell density equals 50% of the normal packing density $c^{(norm)}$. Its cutting planes are slightly offset from those of the vessel network in order to make slices of the tumor vasculature visible. Necrotic regions appear in (c) and (d) as shadowy holes in the viable tumor mass.

Figure 3: Displays final configurations for (a) a 2d system with a regular initial network, at t = 1000 h. The lateral size of the simulation domain is 5.1 mm. (b) a 2d system with an arterio-venous network based on a hexagonal lattice at t = 1200 h. The domain is 12 mm wide and ca 10 mm high. (c) a 3d system with a regular network at t = 400 h. The domain size is 4 mm. The tumor is not displayed here. See (Lee, Bartha and Rieger 2006) for a complete display. (d) the 3d arterio-venous system emergent at t = 600 h from the earlier stages shown in Fig.2. The length of the scale bar represents approximately 1 mm. The tumor is depicted as yellow mass except in (c). In (a) the age of individual tumor cells is indicated by their brightness (darker means older). Vessels are depicted as line segments or cylinders with the corresponding width or radius. Their color indicates the their flow rate q. The color scale in (b) and (d) is identical and stated in Fig.2. The flow rate in (a) is shown on a linear scale ranging from 0 (green) over the value of the flow rate in the undisturbed initial network (which is equal for all initial vessels) (blue) to the maximum flow rate (red). See (Bartha and Rieger 2006) for details. The color scale in (c) ranges from $q = 0$ (dark-cyan) to ∞ (red). See (Lee, Bartha and Rieger 2006) for details.

Figure 4: Shows radial distributions obtained from 3d systems with arterio-venous initial vessel networks (Welter and Rieger 2010). Similar data for other systems can be found in (Bartha and Rieger 2006; Lee, Bartha and Rieger 2006; Welter, Bartha and Rieger 2009). The shown quantities are (a) vessel radius (MVR), (b) microvascular density (MVD), (c) blood flow rate through the vessels, (d) vessel wall shear force, (e) growth factor concentration and (f) oxygen concentration as a function of the radial distance from the tumor center for different times (legend see top left panel). The broken lines indicate the radial tumor density at the times corresponding to the other quantities shown. All curves are averaged over 40 runs and concentric shells of 100 μm width.

Figure 5: Shows probability distributions for morphological quantities of 2d systems with arterio-venous initial networks. In (a) the local MVD, given as the local average over 250 μm wide boxes, (b) the volume of necrotic tissue clusters, defined as the number of sites in connected components of dead tissue. (c) the volume of vessel hot-spot areas, defined as the connected components of regions where the local MVD exceeds a prescribed threshold (ca. the MVD in the initial vasculature). The curves are generated from data collected from results of 40 simulation runs at t = 1200. We note that the distributions show algebraic decay. In this instance in particular with the same exponent with an error of 2%.

Figure 6: Shows a comparison of the local gradient magnitude $|\nabla p|$ of the continuous field $p(\mathbf{r})$ which interpolates the blood pressure between neighboring vessels of an initial network configuration (see text). $|\nabla p|$ is relevant for the survival of neovasculature because the shear stress within a new connection generated between two original vessels is approximately determined by $|\nabla p|$. Therefore the fluctuations in p and $|\nabla p|$ can have an impact on the emergence of inhomogeneities in the tumor vasculature. The gray level of the images correspond to the range between the minimum (white) and maximum (black) $|\nabla p|$ values. (a) Shows the result for a 2d arterio-venous obtained by Welter, Bartha and Rieger (2009), (b) shows a slice through the center of a 3d arterio-venous system and (c) also shows a 3d arterio-venous system but with deterministically laid out parent vessels, mimicking the 2d configurations like shown in (a) more closely.

Figure 7: Visualizes the drug concentration c obtained from a flow simulation at times t = 0.5 s, 1 s, 2 s and 4 s. The left column shows 0.6 mm thick slices through the system center. The right column shows perspective views of cuts through the simulation domain. The scale bar represents approximately 1 mm and the size of the simulation domain is 6 mm. The color code ranges from 0 (gray) to the injected concentration $c = 1$ (red). The transport is very effective since already at t = 4 s the vasculature is mostly saturated.

Table 1: List of parameter values used for all simulations

Parameter	Value	Description
N	600	Lattice size
Δl	10 μm	Lattice const.
Δl_V	60 μm	Lattice const. (tree constr.)
D	300 μm^2 / s	TC mobility
$c^{(norm)}$	1 / (10 μm)^3	Normal cell density
$c^{(max)}$	2 / (10 μm)^3	Maximum cell density
$o^{(B)}$	1	Blood oxygen level
α_o	0.004 /μm^2	O_2 source coefficient
$\gamma_o^{(norm)}$	1/(100 μm)^2	O_2 consumption. coeff. by normal cells
$\gamma_o^{(tum)}$	2/(100 μm)^2	O_2 consumption. coeff. by tumor cells
R_g	200 μm	Growth factor diffusion range
$t_{EC}^{(switch)}$	24 h	Sprouting/Dilation switch delay
$t_{EC}^{(sprout)}$	5 h / 10 μm	Sprout extension time
$t_{EC}^{(migr)}$	100 h	Sprout activity duration
$l^{(spr)}$	20 μm	Sprout sites minimum separation
$r^{(sprout)}$	4 μm	Initial sprout vessel radius
k_r	0.4 μm/h	Vessel dilation rate
$r^{(max)}$	25 μm	Maximum dilation radius
$t_{TC}^{(prol)}$	10 h	TC proliferation time
$t_{TC}^{(uo)}$	100 h	Hypoxic TC survival time
$f^{(coll)}$	2 Pa	Critical wall shear-stress
$t_{EC}^{(coll)}$	20 h	Unstable vessel survival time
Δw	0.05 μm/h	Dematuration (w) rate
$o_{TC}^{(death)}$	0.01	TC death O_2 threshold
$o_{TC}^{(prol)}$	0.1	TC hypoxia O_2 threshold

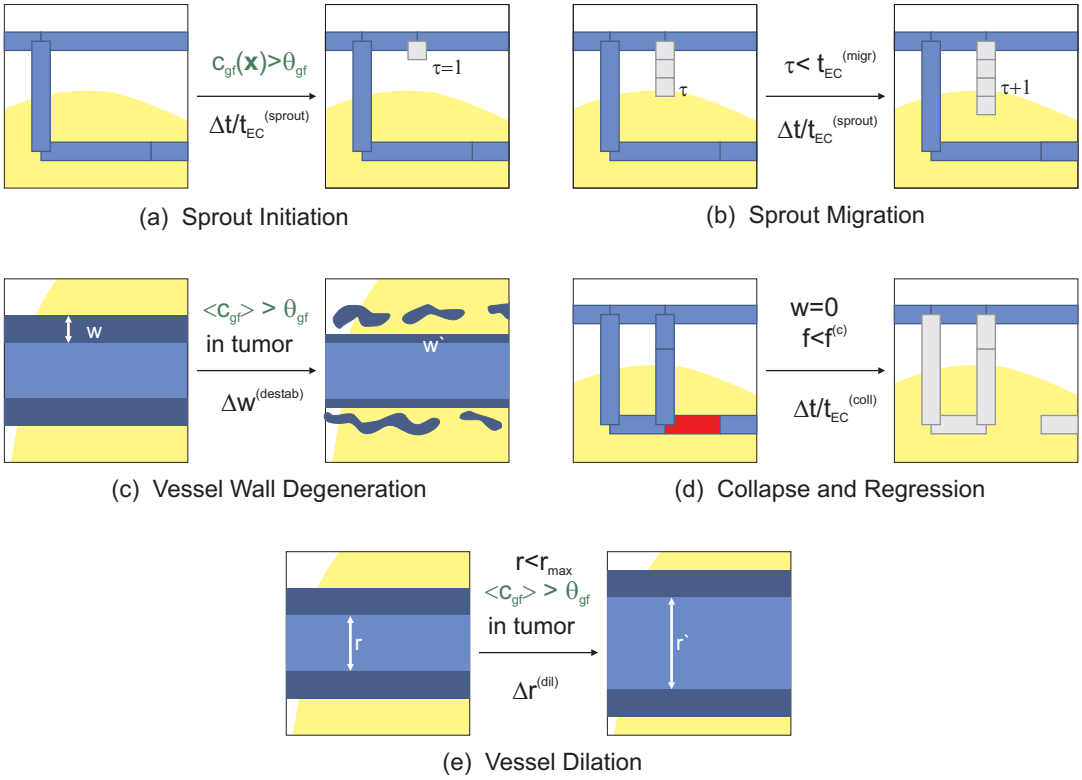
$c_{gf}(\mathbf{x})>\theta_{gf}$
$\Delta t/t_{EC}^{(sprout)}$
τ=1
τ
$\tau< t_{EC}^{(migr)}$
$\Delta t/t_{EC}^{(sprout)}$
τ+1
(a) Sprout Initiation
(b) Sprout Migration
w
$<c_{gf}> > \theta_{gf}$
in tumor
$\Delta w^{(destab)}$
w`
w=0
$f<f^{(c)}$
$\Delta t/t_{EC}^{(coll)}$
(c) Vessel Wall Degeneration
(d) Collapse and Regression
r
$r<r_{max}$
$<c_{gf}> > \theta_{gf}$
in tumor
$\Delta r^{(dil)}$
r`
(e) Vessel Dilation

Fig. 1

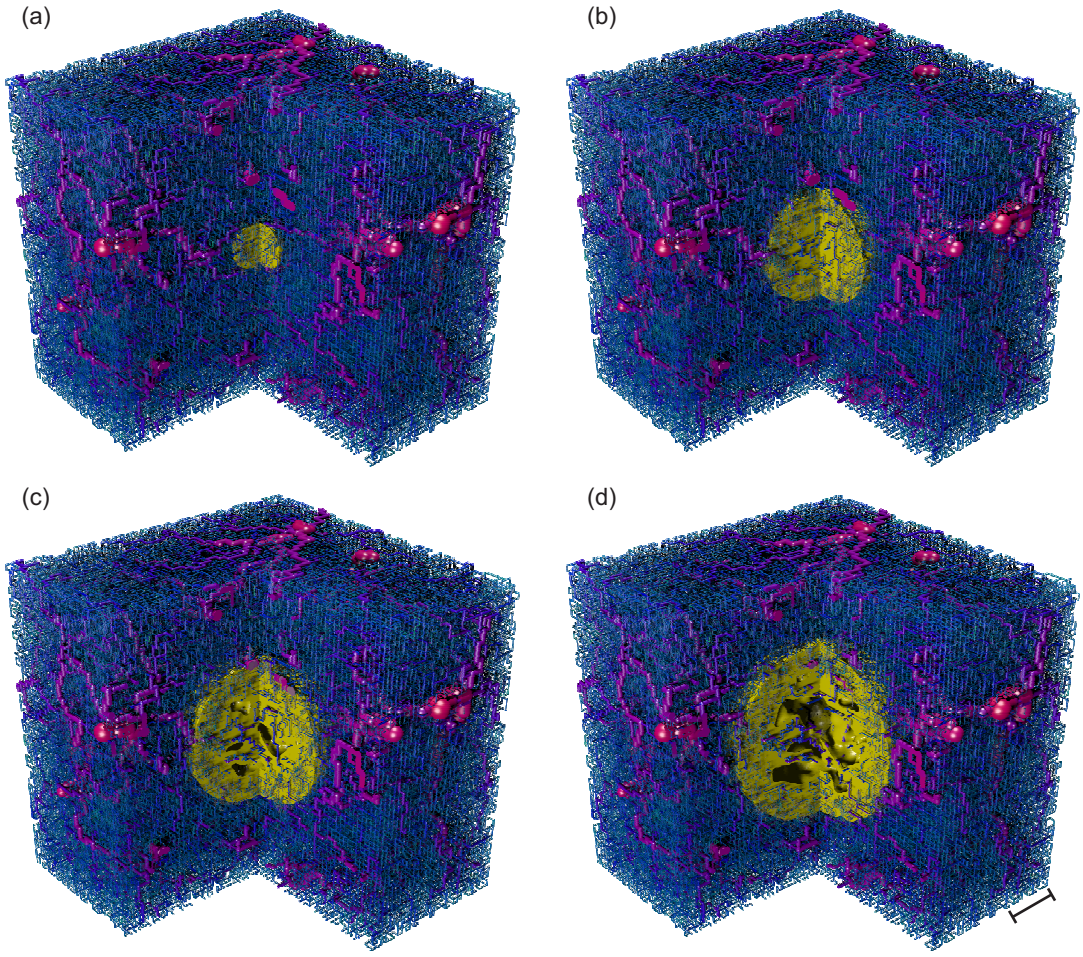

Fig. 2

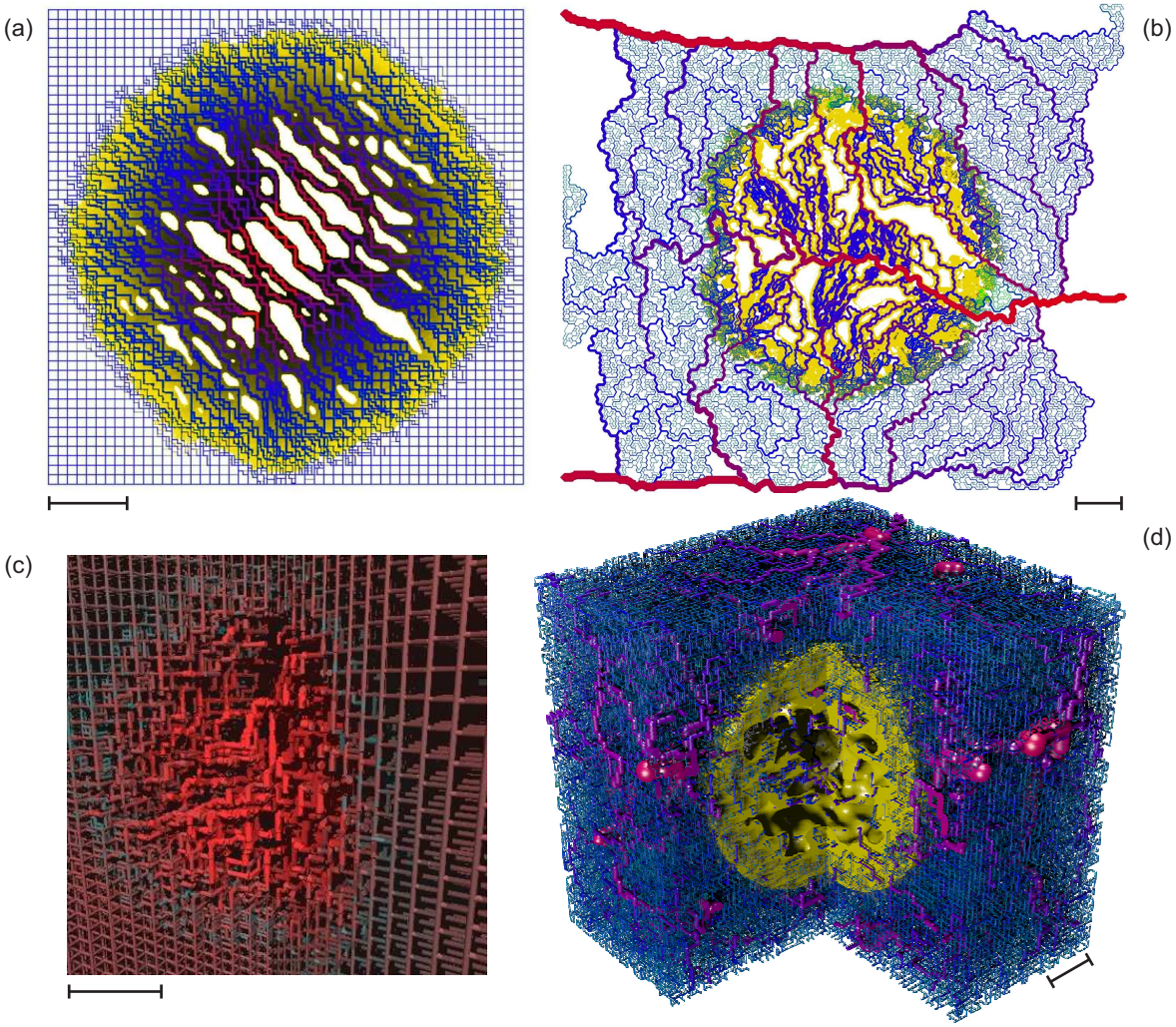

Fig. 3

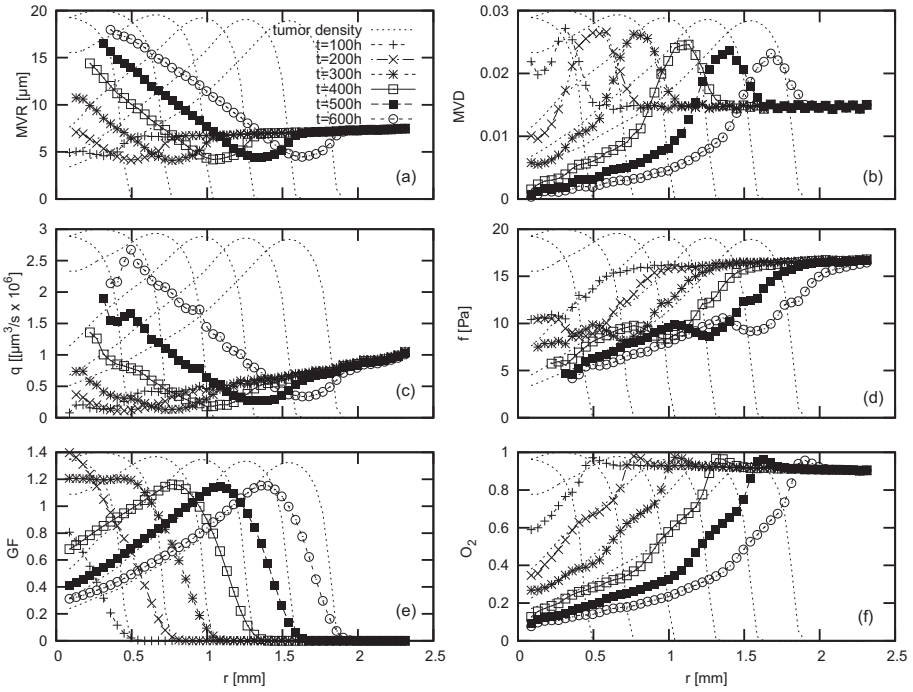
tumor density
t=100h
t=200h
t=300h
t=400h
t=500h
t=600h
MVR [µm]
MVD
q [[µm³/s x 10⁶]
f [Pa]
GF
O2
r [mm]
r [mm]
(a)
(b)
(c)
(d)
(e)
(f)

Fig. 4

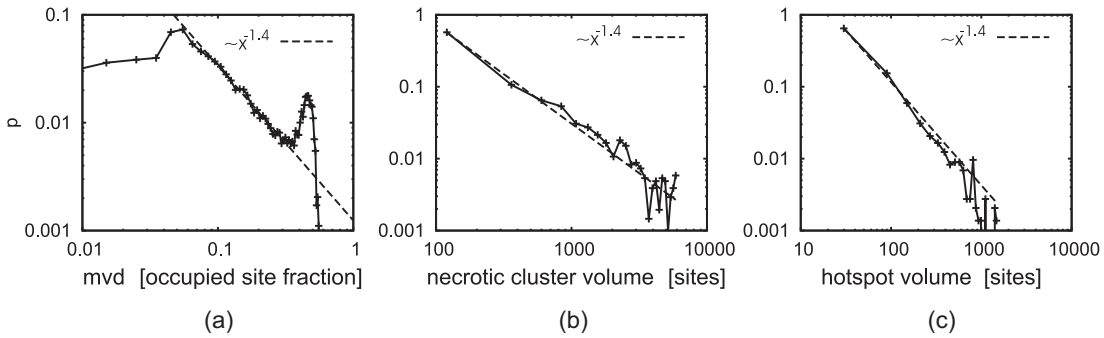
0.1
0.01
0.001
p
0.01
0.1
1
mvd [occupied site fraction]
(a)
1
0.1
0.01
0.001
100
1000
10000
necrotic cluster volume [sites]
(b)
1
0.1
0.01
0.001
10
100
1000
10000
hotspot volume [sites]
(c)

Fig. 5

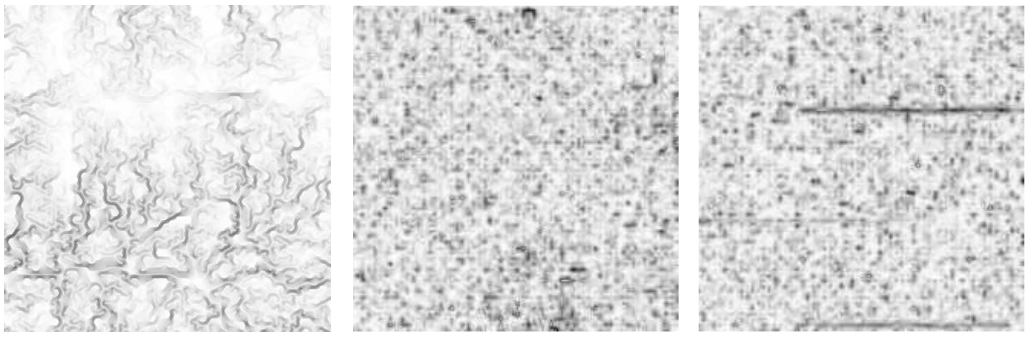

Fig. 6

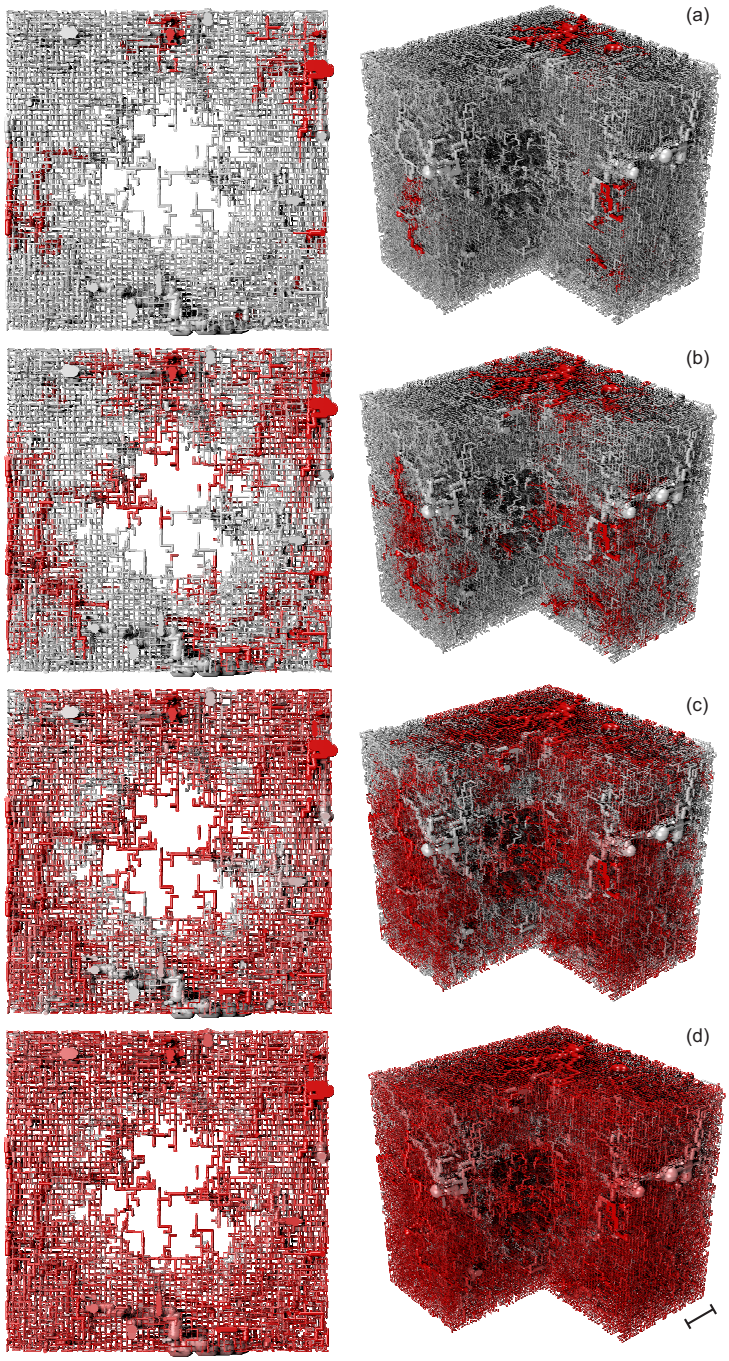

Fig. 7